Research Article

Journal of RAMAN SPECTROSCOPY

Received: 22 June 2010 Accepted: 14 October 2010 Published online in Wiley Online Library:

(wileyonlinelibrary.com) DOI 10.1002/jrs.2843

Correction of optical distortions in dry depth profiling with confocal Raman microspectroscopy

J. Pablo Tomba,* María de la Paz Miguel and Claudio J. Perez

We present a generalized approach to obtain improved Raman intensity profiles from in-depth studies performed by confocal Raman microspectroscopy (CRM) with dry objectives. The approach is based on regularized deconvolution of the as-measured confocal profile, through a kernel that simulates optical distortions due to diffraction, refraction and collection efficiency on the depth response. No specific shape or restrictions for the recovered profile are imposed. The strategy was tested by probing, under different instrumental conditions, a series of model planar interfaces, generated by the contact of polymeric films of well-defined thickness with a substrate. Because of the aforementioned optical distortions, the as-measured confocal response of the films appeared highly distorted and featureless. The signal computed after deconvolution recovers all the films features, matching very closely with the response expected.

Supporting information may be found in the online version of this article.

Keywords: confocal Raman microspectroscopy; depth profiling; depth response; modeling; deconvolution

Introduction

Confocal Raman microspectroscopy (CRM) has widely been shown to be a valuable tool that combines spatially resolved measurements with high sensitivity to molecular, environmental and structural sample features. This natural contrast allows the mapping of the physicochemical features of several families of materials without resorting to chemical labeling and with minimum sample preparation.

One remarkable element of CRM is the capability of in-depth analyses by optical sectioning, i.e. the nondestructive study of thin sample slices as a function of depth. This probing mode, particularly suitable for transparent samples, has naturally found application, for instance, in the polymer field, being applied in studies of distribution of species, crystals or inclusions in a wide variety of matrices.[1–7] In theory, depth (or axial) resolution in confocal conditions is determined by the diffraction-limited laser focal dimensions, which is typically below 2 μm for most of the commercial instruments equipped with visible lasers and high-magnification objectives. However, depth resolution *within* the sample may become refraction-limited, particularly when the laser beam is delivered with dry objectives.[8,9] The mismatch in refractive indices between air and the sample causes significant spreading of the laser focal volume, which results in a dramatic broadening of the depth response as one probes deeper into the sample. Another undesirable effect is that the depth scale is artificially compressed, making sample features appear artificially closer to the microscope objective. Laser refraction also perturbs the collection efficiency of the confocal system, causing a continuous reduction in the detected intensity with focusing depth.[10–12] All these effects conspire against data quality, smearing out important sample details.

In microscopy, the standard way of minimizing the influence of refraction is the use of immersion objectives with a fluid whose refractive index matches that of the sample. However, this strategy is not always viable, as many substrates (e.g. polymers) do not tolerate the direct contact with the organic liquids used as coupling fluids, besides the potential problem of spectral overlapping. A series of instrumental adaptations has been suggested to avoid sample damage, which includes the use of double-oil configurations, objectives with cover slip correction or the reversible application of protective coatings; the reader may refer to Ref. [13] for further details.

In a different direction, data correction through mathematical modeling appears as a wise strategy yet to be explored in CRM. Overall, the core of these methods relies on precise knowledge on how the depth response is distorted by optical/instrumental conditions. Recently, Reinecke *et al*. reported one of the first and remarkable attempts to obtain Raman intensity depth profiles of modifiers in polymer films improved by numerical corrections, where modifier distribution and depth response are obtained by fitting data to pre-established function, with the help of a sample with known profile to calibrate the depth response.[14]

We report here a general approach based on regularized deconvolution, which is designed to recover realistic Raman intensity depth profiles from distorted measurements carried out with dry objectives. The strategy does not assume any specific shape for the recovered profile and uses a simple predictive model to describe the depth response. We test our approach by probing

* *Correspondence to: J. Pablo Tomba, Institute of Materials Science and Technology (INTEMA), National Research Council (CONICET), National University of Mar del Plata, Juan B. Justo 4302, (7600) Mar del Plata, Argentina. E-mail: jptomba@fi.mdp.edu.ar*

Institute of Materials Science and Technology (INTEMA), National Research Council (CONICET), National University of Mar del Plata, Juan B. Justo 4302, (7600) Mar del Plata, Argentina

under different instrumental conditions a series of well-defined planar interfaces generated by contact between polymeric films of well-defined thickness with a substrate. In this model system, the genuine undistorted response is exactly known in advance; on the other hand, the presence of sharp sample features represents a serious challenge to the precision and reliability of the method.

Experimental

Model planar interfaces were produced by contact between a flexible polypropylene (PP) film with a rigid, much ticker poly(methyl methacrylate) (PMMA) piece. The PP film was maintained in position using holders, which were adjusted to apply a slight tensile force on the edges of the film. The PMMA piece had a smooth, carefully polished, convex curvature on the top, which, combined with the tensile force applied to the film borders, produced a good film/substrate contact. PP films with thicknesses of 28, 50 and 80 μm, as measured with a Mitutoyo micrometer (model 395-271, ±1 μm precision), were used.

Raman spectra were recorded on a Renishaw in-Via Reflex spectrometer, equipped with a charge coupled device (CCD) detector of 1024×256 pixels for the spectral and spatial dimensions (26 μm pixel width), a holographic grating of 2400 groves/mm and a 50-mW Ar laser (514 nm wavelength) as excitation source. Confocality is achieved by properly selecting a limited active area on the spatial CCD dimension and by controlling the aperture of the spectrometer slit. Two confocal setups were employed: *high confocality* (optimum depth resolution), which uses three pixels of the CCD detector and 20 μm slit width, and *regular confocality* (optimum signal), via nine pixels of the CCD detector and 65 μm slit width. Data were acquired with two Leica metallurgical objectives with different numerical apertures (NAs): 0.9 (100×) and 0.75 (50×). Depth profiling was carried out by mounting the samples on a microscope stage with vertical displacement, controlled by software, with 0.1 μm precision. Raman intensity depth profiles were measured by recording Raman spectra from different depths by moving the stage vertically (or axially) in steps of 1 μm.

Modeling and Data Treatment

The core of the numerical corrections based on deconvolution is the first kind Fredholm integral equation that relates the *as-measured* (I_m) and *true* (I_r) intensity profiles:

$$I_m(\Delta) = \int_0^{\infty} B(\Delta, z) I_r(z)\, dz \qquad (1)$$

where $B(\Delta, z)$ represents the instrumental point spread function (PSF) which accounts for the contributions to the signal measured at the point Δ, from surroundings located at different depths along the z (axial) coordinate. In depth profiling by CRM, Δ (or nominal focus point) is taken as the sample displacement in the axial direction, as read from the microscope platform scale. Notice that we have followed the notation used in most of the previous work on the topic; see, for instance, Ref. [8,10,12].

To build the PSF, we have followed a semiempirical approach described in an earlier work, which yields a good balance between precision and simplicity.[15] We highlight here the integral and rigorous treatment for diffraction/refraction effects proposed by Sourisseau, but based on a much more complex and computationally demanding formalism.[16] We focus on axial

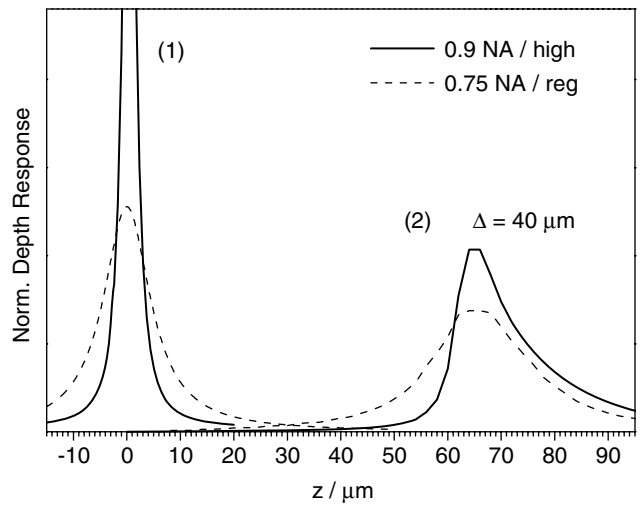

Figure 1. CRM depth responses with dry optics for 0.9 NA (100×) and 0.75 NA (50×) objectives: (1) Lorentzian fits of the measured silicon response for 0.9 NA/high confocality (solid) and 0.75 NA/regular confocality (dashed) combinations; (2) predicted response at a nominal focusing depth of 40 μm for combinations 0.9 NA/high confocality (solid) and 0.75 NA/regular confocality (dashed).

contributions, assuming that orthogonal spreading of the laser beam is minor; however, volume contributions are particularly important near the sample surface, with important implications in surface specificity.[17,18] We start with the depth response in the absence of refraction, characterized by a relatively narrow bell-shaped function, i.e. Lorentzian, centered at Δ, and essentially invariant with focusing depth. We assume that this response, frequently referred to as diffraction, can be well characterized by a standard test in CRM: the depth scanning through the surface of a polished silicon wafer.[8,11,12] Overall, that response depends on the optical setup used. Curves labeled as (1) in Fig. 1 show normalized Lorentzian fittings to experimental data obtained with 0.9/0.75 NA objectives under conditions of high/standard confocality (solid and dashed lines, respectively). We see that the combination of high NA objective/high confocality (or small confocal aperture in pinhole-based instruments) yields a much sharper depth response, 4–5 times narrower, but at the cost of detecting much less Raman scattering, as discussed below.

We include the influence of on-axis laser refraction at the air/sample interface on the original diffraction response by following the treatments developed by Everall and Batchelder. Using simple geometric optics, Everall quantified the deviation of the laser beam when it is focused at Δ, by calculating the true point of focus on the z-axis where it is directed, as a function of n (sample refractive index), NA and m (normalized distance across the lens in radial direction)[8]:

$$z = \Delta \left[m^2 \frac{\mathrm{NA}^2(n^2 - 1)}{1 - \mathrm{NA}^2} + n^2 \right]^{0.5} \qquad (2)$$

Equation (2) predicts that the degree of deviation depends on the position of the ray with respect to the optical axis (m) and that the laser beam illuminates a region instead of a single point; the span of this region (depth of focus, z(m=1) - z(m=0)) is also predicted to increase as one focuses deeper into the material. Assuming that the laser beam illuminates a circular pupil in the microscope lens with a Gaussian radial intensity distribution,

Everall found a simple expression for the illuminated region, $I(m) = mI_0 \exp(-2m^2)$, which, combined with Eqn (1), yields, for a ray originally directed at Δ, the true laser illumination distribution over z.[8,13] In the collection path, part of the Raman scattering that originates from the illuminated region is blocked by the confocal aperture, which restricts the sampled region. To model the effect, we follow the description by Batchelder, who added a factor of collection efficiency (Ω) to the expression for the illuminated region derived by Everall; details of the calculation of Ω as a function of Δ, n, NA and the size of confocal aperture can be found elsewhere.[10] The well-documented overestimation in the decay rate predicted by Batchelder is corrected here through a renormalization from independent experiments on thicker PP films with similar transparency, as detailed elsewhere.[12,15] Curves labeled as (2) in Fig. 1 show the predicted depth responses that result from the combined effects of diffraction and refraction. Calculations correspond to 0.9/0.75 NA objectives in conditions of high/standard confocality, for a nominal focusing depth of 40 µm. We see that depth responses lie much deeper than the point where the laser beam was originally focused (Δ) and that they span over much wider regions than the original diffraction-limited response shown by curves (1).

In order to obtain the true (or corrected) Raman response from Eqn (1), $I_m(\Delta)$ and $I_r(z)$ are discretized as two vectors $\boldsymbol{I}_m = [I_m(\Delta_1), I_m(\Delta_2) \ldots I_m(\Delta_{n_1})]^{\mathrm{T}}$ and $\boldsymbol{I}_r = [I_r(z_1), I_r(z_2) \ldots I_r(z_{n_2})]^{\mathrm{T}}$ in such a way that Eqn (1) can be written as

$$\boldsymbol{I}_m = \boldsymbol{B}\,\boldsymbol{I}_r \tag{3}$$

where $\boldsymbol{B}$ is an $(n_1 \times n_2)$ matrix, whose values depend on the expressions used for PSF and on the quadrature formula used in the discretization.

Direct least squares solution of Eqn (3) implies the minimization of the functional $J(\boldsymbol{I}_r) = |\boldsymbol{I}_m - \boldsymbol{B}\,\boldsymbol{I}_r|^2$ with respect to $\boldsymbol{I}_r$, which yields $\boldsymbol{I}_r = (\boldsymbol{B}^{\mathrm{T}}\boldsymbol{B})^{-1}\ \boldsymbol{B}^{\mathrm{T}}\ \boldsymbol{I}_m$ as solution. However, because of the ill-conditioning characteristics of this type of problems, the solution $\boldsymbol{I}_r$ shows dramatic oscillations, which make it practically useless. To minimize distortions in order to recover a meaningful profile, we resort to regularizing the solution via the so-called Philips–Thikonov technique.[19] The method introduces a penalty function (q) and a regularization parameter (γ) to the original formulation in such a way that the functional to be minimized turns out as $J(\boldsymbol{I}_r) = |\boldsymbol{I}_m - \boldsymbol{B}\,\boldsymbol{I}_r|^2 + \gamma\ q\ (\boldsymbol{I}_r)$. The function q must be large for oscillatory solutions and small for smooth ones. Usually, q is selected as the sum of the squares of the second differences of $\boldsymbol{I}_r$[19,20]; in this work, we have introduced a slight modification given by the parameters γ_i, whose significance will be discussed below. The explicit form of q used is then given by

$$q(\boldsymbol{I}_r) = \sum_{j=2}^{n_2-1} (2\gamma_{j-1} I_{r_j} - I_{r_{j-1}} - I_{r_{j+1}})^2 = \boldsymbol{I}_r^{\mathrm{T}}\,\boldsymbol{K}^{\mathrm{T}}\,\boldsymbol{\Gamma}\boldsymbol{K}\,\boldsymbol{I}_r \tag{4}$$

where the last term on the right-hand side corresponds to the matrix form notation. In this form, $\boldsymbol{K}$ is a tridiagonal matrix, with elements '2' in the main diagonal and '−1' in the other two, while Γ, a diagonal matrix, only contains the 'γ_i' elements. With the inclusion of the penalty function, the solution for the minimization problem is now given by

$$\boldsymbol{I}_r = (\boldsymbol{B}^{\mathrm{T}}\boldsymbol{B} + \gamma\ \boldsymbol{K}^{\mathrm{T}}\ \boldsymbol{\Gamma}\boldsymbol{K})^{-1}\boldsymbol{B}^{\mathrm{T}}\,\boldsymbol{I}_m \tag{5}$$

The γ parameter determines the amount of regularization (smoothing) on the solution sought. With $\gamma = 0$, no regularization is applied and Eqn (5) yields the highly noisy least squares solution; with $\gamma > 0$, abrupt oscillations in the solution are suppressed. One important point is that regularization may mask important sample features, such as, abrupt changes of intensity in edges, interfaces or phase transitions. In order to avoid this effect, we ponder the relative amount of regularization along the z coordinate via the Γ matrix. The elements of Γ make regularization strong where the signal is presumed to be smooth and weak where the signal changes rapidly, i.e. edges, interfaces and transitions. Thus, the diagonal elements of Γ, $\gamma_1, \gamma_2, \ldots, \gamma_{n2}$, are sampled from $\gamma_i = 1 - \mathrm{e}^{-(i-z_\gamma)^2}/2\sigma_\gamma^2$, where z_γ is the row of Γ that corresponds to the maximum change of the reconstructed signal. σ_γ measures how fast regularization increases to both sides of the center z_γ, or point of maximum change. Thus, for $i = z_\gamma$, regularization is null, while for values of i far from z_γ the elements of Γ tend to 1, allowing maximum regularization.

In the treatment of real data, the regularization conditions are chosen as follows. To find the center of the regularization function (z_γ), we identify the points of maximum change in the original signal, measured on the Δ scale, from its first derivative. To place z_γ on the z scale, those values are multiplied by a factor that accounts for the apparent compression shown by Δ due to refraction. This correction factor can be obtained by simulating the apparent position of a known sample feature via Eqn (1); for a material with $n = 1.5$ scanned in air, a value of 1.7 was found, which agrees with experimental observations.[13] For σ_γ, we found that values between 10 and 20 usually yielded good results. To find the optimum amount of regularization, i.e. the value for γ, we follow the well-established generalized cross validation (GCV) technique, whose details are given elsewhere.[21] GVC computes a lower bound for γ according to each experiment as the one that minimizes the following function:

$$V(\gamma) = \frac{|(\boldsymbol{I} - \boldsymbol{Z})\,\boldsymbol{I}_m|^2}{|\mathrm{Trace}\ (\boldsymbol{I} - \boldsymbol{Z})|^2} \tag{6}$$

where $\boldsymbol{Z} = \boldsymbol{B}\,(\boldsymbol{B}^{\mathrm{T}}\boldsymbol{B} + \gamma\ \boldsymbol{H})\boldsymbol{B}^{\mathrm{T}}$ and $\boldsymbol{I}$ is the identity matrix.

Results and Discussion

Figure 2(a)–(c) shows the raw Raman intensity profiles of a 50-µm thick PP film, as depth-scanned through air for several combinations objective/confocality as indicated. To construct these profiles, we applied methods of analysis based on processing the complete Raman spectrum, i.e. linear decomposition or component analysis,[22] which yields data much less noisy and more suitable for our analysis than those obtained by plotting the intensity of a single band. The abscissa scale corresponds to the nominal focusing depth Δ, as determined from the microscope stage position, where the zero corresponds to the PP film outer surface. The confocal profiles of Fig. 2 show the typical features of depth profiling experiments with dry objectives. Raman intensity starts from a value near zero when the focal volume is in air, and rapidly increases when it passes through the sample surface and is finally well within the sample. Fine details of this increase reflect the different combinations of objective/confocality employed. Once the nominal focus point is within the sample, Raman intensity progressively decreases till it reaches the interface with the PMMA substrate. The planar PP/PMMA interfaces, which should appear as a sharp transition, are shown instead as an artificially broadened region. The apparent film thicknesses obtained from any of these experiments

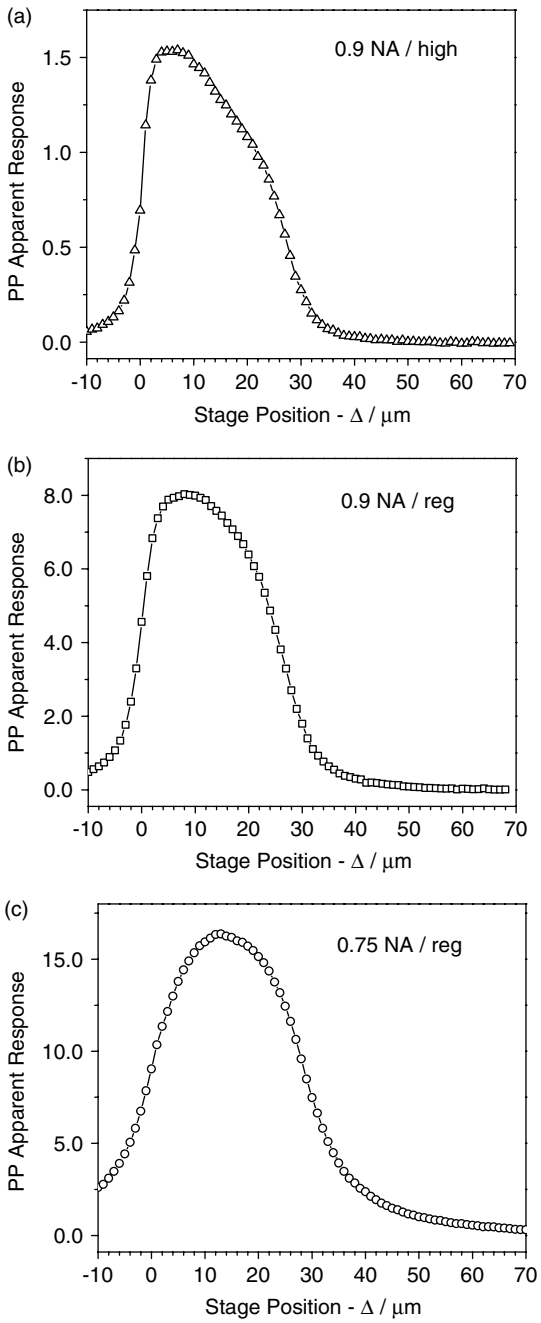

Figure 2. As-measured Raman intensity profiles for the 50-μm thick PP film, for the instrumental combinations objective/confocality indicated in each plot.

are roughly two times smaller than those expected on the basis of its nominal value. Notice that, as seen on the intensity axis (y), the experiment that used the 0.75 NA/regular conditions yielded ten times more Raman scattering than the 0.9 NA/high combination.

These raw confocal profiles were deconvoluted with the proposed methodology to obtain the corrected response $\boldsymbol{I}_r$. To find the solution of Eqn (3) via Eqn (4), we need $\boldsymbol{I}_m$ and PSF as inputs. The series of n_1 nodal values for each Δ_i that constitutes $\boldsymbol{I}_m$ were taken as each of the points of the experimental intensity profile, as acquired. The number of nodal z_i values at which the corrected signal is evaluated, n_2, was taken as equal to n_1. As the compression effect of the true coordinate is more roughly by a factor of 2, i.e. 1-μm interval in the Δ scale is equivalent to about 2 μm in z, nodal values in the z coordinate were spaced by steps of 2 μm. Discrete values of PSF in the z domain for each Δ_i value were calculated as described above, starting from the diffraction contribution (Lorentzian fittings of the silicon experiment), which is further distorted via convolution with the models that simulate refraction. The integrals for these calculations were solved by Simpson's rule with 0.1-μm steps. We took $n = 1.50$ for the polymer medium and NA values of 0.9 and 0.75 for each of the objectives; the radius of confocal apertures were taken as 1.0/3.0 μm (0.9 NA objective) and 2.0/6.0 μm (0.75 NA objective) for conditions of high/regular confocality, respectively.[10] The regularization parameters were chosen as follows. Two points of maximum change, i.e. values for z_γ, were selected in correspondence with the air/sample ($z_\gamma = 0$ μm) and PP/PMMA ($z_\gamma \sim 50$ μm) interfaces. These values were obtained from the first derivative of the raw profile and translated to the z domain as explained earlier. σ_γ in the range 10–20 μm yielded good results although the recovered profile was not found to be very sensitive to this parameter. The application of the GCV method yielded a lower bound for γ in the range 2–10; representative curves for $V(\gamma)$ are shown in Fig. S1 (Supporting Information). Overall, these values are a rather good estimation of γ and provide a nice quality of data reconstruction. However, in some cases, somewhat better results were obtained with larger γ values (10–100 range), which is not surprising, as GVC tends to slightly underestimate the optimum amount of regularization.[20]

Figure 3(a)–(c) shows the corrected Raman intensity profiles of PP, that is, the elements of $\boldsymbol{I}_r$. Notice that the depth scale is now labeled as z, the true axis coordinate. We have also included boxcar functions representing the expected (true) profile. We see that the main film features are very well recovered: the air/PP and PP/PMMA interfaces are now very sharp and connected by a region of fairly constant intensity, with minimum spurious oscillations that are typical of the problem inversion. Overall, we see that the recovered signal matches those expected and represented by the boxcar functions very closely, and that the film thickness, determined as the range of depths between interfaces, matches very well with the nominal value, i.e. 50 μm. Remarkably, the same good agreement is seen for all the instrumental configurations, including experiments carried out in technically poor confocal conditions, i.e. 0.75 NA/regular combination.

Conclusions

This work has shown that it is possible to use mathematical corrections to obtain realistic Raman depth profiles from data highly distorted by optical aberrations, preserving the highly convenient noncontact features of the probing technique. The strategy requires a minimum set of inputs, some of them operative and others obtained from independent experiments; the last point basically avoids detailed modeling of the particular optical setup of each instrument, for the benefit of a more generalized approach. As no assumptions are made about the nature of the profile to be processed, it can be used to correct any other type of transitions, for instance, diffusion profiles with sharp features. We have also seen that the quality of the reconstructed data does not depend much on the acquisition conditions, which allows measurements in poor confocal conditions without loss in precision, an important aspect also pointed out by other researchers.[14]

One limitation of the methodology is the assumption of uniform refractive index for the sample, which might limit

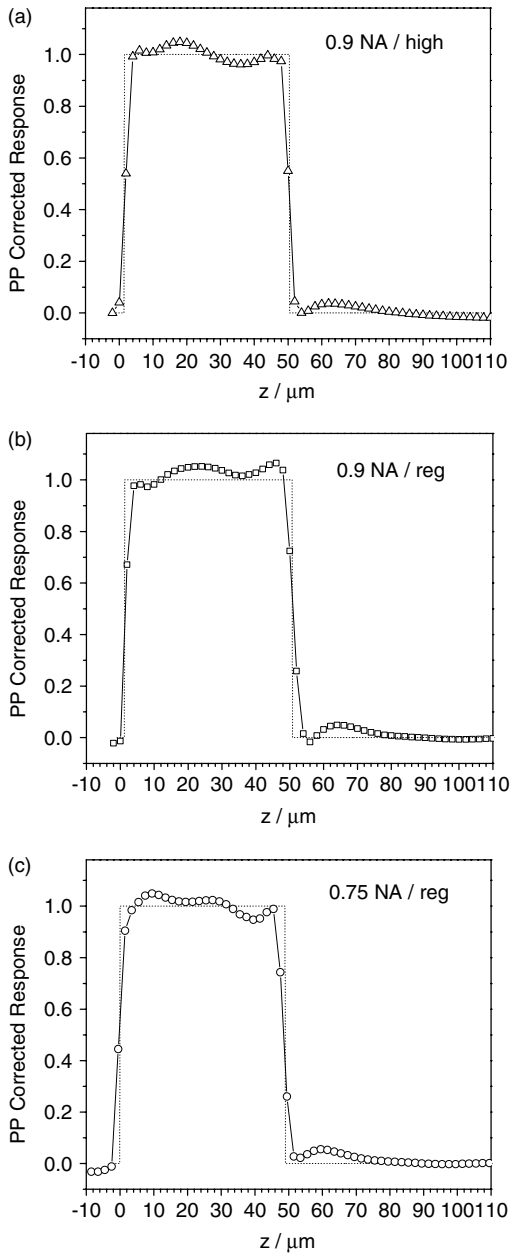

Figure 3. Corrected Raman intensity profiles for the PP film obtained after regularized deconvolution of the data in Fig. 2. Inputs: Lorenztian fits as indicated in Fig. 1 (1), $n = 1.50$, NA values of 0.9 and 0.75 for 100× and 50× objectives, respectively; radius of confocal apertures of 1.0/3.0 µm (0.9 NA) and 2.0/6.0 µm (0.75 NA) for high/regular confocality respectively; σ_γ in the range 10–20 µm; $\gamma = 10$ for 0.9 NA/high and 0.75 NA/high; $\gamma = 10^2$ for 0.9 NA/reg. The dotted lines represent boxcar functions with widths of 49.0 (a), 49.5 (b) and 49.0 (c) µm.

the analysis of complex, heterogeneous substrates with large variations in that property. However, there exists a vast range of transparent materials susceptible to be depth-profiled (e.g. polymers) with n values narrowly distributed around 1.5. The use of the methodology to trace the distribution of species (i.e. additives, modifiers) in a host matrix can be safely carried out, assuming that the presence of those species does not change the average refractive index appreciably. Although the results found are encouraging, and could be extended to the other films examined but not shown here, we believe that an even better quality of data reconstruction can be achieved using more refined approaches to describe optical aberrations, which are able to model, for instance, off-axis contributions.

Supporting information

Supporting information may be found in the online version of this article.

Acknowledgements

This work is part of a project funded by ANPCYT (PICT06-1359). The confocal Raman microscope was acquired with funds from ANPCYT and CONICET (PME06-2170). Helpful discussions with Dr. Richard Bormett (Renishaw Inc.) are acknowledged.

References

[1] J. P. Tomba, L. Arzondo, J. M. Carella, J. M. Pastor, *Macromol. Chem. Phys.* **2007**, *208*, 1110.
[2] L. Arzondo, L. J. P. Tomba, J. M. Carella, J. M. Pastor, *Macromol. Rapid Commun.* **2005**, *26*, 632.
[3] O. S. Fleming, F. Stepanek, S. G. Kazarian, *Macromol. Chem. Phys.* **2005**, *206*, 1077.
[4] B. Marton, L. G. J. van der Ven, C. Otto, N. Uzunbajakava, M. A. Hempenius, G. J. Vansco, *Polymer* **2005**, *46*, 11330.
[5] F. Belaroui, Y. Grohens, H. Boyer, Y. Holl, *Polymer* **2000**, *41*, 7645.
[6] J. Sacristan, H. Reinecke, C. Mijangos, S. Spells, J. Yarwood, *Macromol. Chem. Phys.* **2002**, *203*, 678.
[7] A. M. Macdonald, A. S. Vaughan, P. Wyeth, *J. Raman Spectrosc.* **2002**, *33*, 815.
[8] N. Everall, *Appl. Spectrosc.* **2000**, *54*, 1515.
[9] N. Everall, *Appl. Spectrosc.* **2000**, *54*, 773.
[10] K. J. Baldwin, D. N. Batchelder, *Appl. Spectrosc.* **2001**, *55*, 517.
[11] J. L. Bruneel, J. C. Lassegues, C. Sourisseau, *J. Raman Spectrosc.* **2002**, *33*, 815.
[12] J. P. Tomba, J. M. Pastor, *Vib. Spectrosc.* **2007**, *44*, 62.
[13] N. Everall, *Appl. Spectrosc.* **2009**, *63*, 245A.
[14] A. Gallardo, S. Spells, R. Navarro, H. Reinecke, *J. Raman Spectrosc.* **2007**, *38*, 880.
[15] J. P. Tomba, L. Arzondo, J. M. Pastor, *Appl. Spectrosc.* **2007**, *61*, 177.
[16] C. Sourisseau, P. Maraval, *Appl. Spectrosc.* **2003**, *57*, 1324.
[17] N. Everall, *Appl. Spectrosc.* **2008**, *62*, 591.
[18] A. M. Macdonald, A. S. Vaughan, *J. Raman Spectrosc.* **2007**, *38*, 584.
[19] D. L. Phillips, *J. Assoc. Comp. Mach.* **1962**, *9*, 84.
[20] G. E. Eliçabe, L. García Rubio, *Adv. Chem. Ser.* **1990**, *227*, 83.
[21] G. H. Golub, M. Heath, G. Wahba, *Technometrics* **1979**, *21*, 215.
[22] J. P. Tomba, *J. Polym. Sci., Part B: Polym. Phys.* **2005**, *43*, 1144.

